Atmos. Chem. Phys. Discuss., 6, 2897–2922, 2006
www.atmos-chem-phys-discuss.net/6/2897/2006/

Atmospheric Chemistry and Physics Discussions

Optical properties and mineralogical composition of different Saharan mineral dust samples: a laboratory study

C. Linke[1], O. Möhler[1], A. Veres[2], Á. Mohácsi[3], Z. Bozóki[3], G. Szabó[2], and M. Schnaiter[1]

[1]Forschungszentrum Karlsruhe, Institute of Meteorology and Climate Research, P.O. Box 3640, 76021 Karlsruhe, Germany
[2]University of Szeged, Faculty of Natural Sciences, Department of Optics and Quantum Electronics, P.O. Box 406, 6701 Szeged, Hungary
[3]Research Group on Laser Physics of the Hungarian Academy of Sciences, Dóm tér 9., 6720 Szeged, Hungary

Received: 23 December 2005 – Accepted: 7 February 2006 – Published: 11 April 2006

Correspondence to: M. Schnaiter (martin.schnaiter@imk.fzk.de)

Abstract

In aerosol chamber experiments optical properties of airborne mineral dust samples of defined size distribution were measured. Extinction coefficients (b_{ext}) and mass specific extinction cross sections (σ_{ext}) were determined for Saharan dust samples from different locations. The results for σ_{ext} were not very sensitive to the type of dust and varied at λ=550 nm between 3.3±0.4 $m^2\,g^{-1}$ and 3.7±0.4 $m^2\,g^{-1}$. The absorption coefficients (b_{abs}) and mass specific absorption cross sections (σ_{abs}) were determined with a novel multi-wavelength photo-acoustic absorption spectrometer (PAS). Between λ=266 nm and λ=1064 nm the derived single scattering albedos (SSA) ranged from 0.63±0.04 to 0.99±0.01. Additionally the chemical and mineralogical composition of the dust samples was analysed with special regard to the iron oxide phases hematite and goethite. At λ=266 nm the mineral dust sample without any detectable iron oxides showed a significantly higher SSA compared to the sample with a hematite content of 0.6 wt-%.

1 Introduction

Mineral dust aerosols from desert regions contribute significantly to the total atmospheric aerosol load (Andreae, 1995). During the transport over long distances depending on their atmospheric residence time the dust clouds are able to affect the earth's radiative budget by absorption and scattering in the near-UV, visible and infrared spectral regions. The optical properties vary with size and mineralogical composition of the dust, resulting in a positive or negative radiative forcing by the aerosol. Especially dark mineral phases like iron oxides predominantly influence the wavelength-dependent mass specific absorption cross section of naturally occurring mineral dusts in the visible spectral region (Tegen et al., 1996; Sokolik and Toon, 1999).

We measured the specific extinction and absorption cross-sections of different airborne Saharan dust samples in the UV/VIS spectral region. All optical instruments

sampled from a laboratory aerosol chamber which contained the mineral dust aerosol with a well characterised size distribution in the sub-micron particle diameter range.

Spectra of the extinction coefficient were measured from λ=230 to 1000 nm. The absorption coefficient and, hence, the single scattering albedo were determined at three wavelengths in the near-UV (λ=266 nm), the visible (λ=532 nm), and the near-IR (λ=1064 nm). In addition to the optical measurements, the chemical and mineralogical compositions of the dust samples were analysed, with a focus on iron oxide mineral phases, i.e. hematite (Fe_2O_3) and goethite (FeO(OH)). The correlation between the deduced spectral quantities and the iron oxide content of the samples is discussed.

2 Aerosol chamber experiments

2.1 Experimental set-up

The experiments were conducted at the stainless steel aerosol chamber NAUA which is part of the AIDA (Aerosol Interactions and Dynamics in the Atmosphere) facility of Forschungszentrum Karlsruhe, Germany. The chamber has a volume of 3.7 m^3 which allows measurements over several hours with the suite of devices used in this study (Fig. 1). The chamber is equipped with a mixing fan for homogeneous conditions throughout the chamber volume. A synthetic air flow of about 2 $m^3\,h^{-1}$ assures a constant dilution rate of the aerosol during the experiment.

Mineral dust aerosol was generated and added to the aerosol chamber by roughly dispersing the finest sieved fraction (<20 μm) of the dry desert dust samples in a rotating brush disperser (Palas, RGB 1000), de-agglomerating the finest particles in an aerosol dispersion nozzle and removing larger particles in a series of four 90° inertial impactor stages with a cutoff $d_{(50)}$ of 1.2 μm. Both the brush disperser and the dispersion nozzle were operated with dry and particle-free synthetic air. The dispersion pressure of the nozzle was 1.5 bar.

The extinction coefficient was measured wavelength-resolved from λ=230 to

1000 nm with a spectral resolution of 2.5 nm by the extinction spectrometer LOPES (Schnaiter et al., 2005). The optical cell of LOPES is a horizontally mounted stainless steel flow tube of 3.5 m length and of 26 mm inner diameter. The optical length is twice the geometric length. The tube was operated at a flow rate of 5 $L\,min^{-1}$ resulting in an aerosol transmission efficiency of more than 95% for particles with diameters smaller than 1 μm.

Absorption measurements were conducted with a multi-wavelength photo-acoustic absorption spectrometer (PAS) recently developed at the University of Szeged, Hungary, with a total flow rate of 1.5 $L\,min^{-1}$. PAS uses the fundamental (λ=1064 nm), the frequency doubled (λ=532 nm), and quadrupled (λ=266 nm) modulated emission of a diode-laser-pumped, quasi-continuous wave, Q-switched Nd:YAG laser (Spectra Physics, laser head VHP80-106Q, power supply J20I-8S40-16NSI) for the photoacoustic signal generation, which basically implies the conversion of light into acoustic energy. The intensity of the generated sound, which was detected with a microphone placed inside a resonant PA cell, is proportional to the concentration of absorbing trace molecules or aerosol particles. The Nd:YAG laser was run at 16 kHz repetition rate (which was the optimum frequency for the highest fourth harmonic power) and was modulated with 4 kHz (which was equal with the resonance frequency of the PA cells). The wavelength conversion was achieved by focusing first the near-infrared light (1064 nm) to a nonlinear LBO (LiB_3O_5) crystal followed by focusing the derived green light to a second nonlinear DKDP (deuterated potassium dihydrogen phosphate) crystal. The power of the laser lights were 750 mW @1064 nm, 80 mW @532 nm and 4 mW @ 266 nm. This system is an upgraded version of an earlier one used for photoacoustic ozone detection (Veres et al., 2005). While the ozone detection system used only one photoacoustic cell, through which the 266 nm wavelength laser was sent, the present system uses 3 identical PA cells each of which illuminated with one of the 3 different wavelengths. Aerosol sampled from the chamber was split off into three identical flows through the PA cells.

To determine the absorption coefficients at λ=266 nm and λ=532 nm the photo-

acoustic cells were calibrated with ozone and NO_2, respectively. For the ozone calibration at λ=266 nm a cross section of 9.44×10^{-18} cm^2/molecule was applied, taken from a spectrum by Voigt et al. (2001) measured at 293 K and 1000 mbar. For the NO_2 calibration at λ=532 nm a cross section of 1.47×10^{-19} cm^2/molecule was used, taken from a spectrum by Voigt et al. (2002) which was also measured at 293 K and 1000 mbar.

At the IR-wavelength λ=1064 nm the PAS system was calibrated with soot from a co-flow diffusion flame of propane and air (Combustion Aerosol Standard, CAST, Jing-CAST Technologies). The burner was operated at a C/O ratio of 0.29. Wavelength-dependent mass-specific absorption cross sections of the same CAST-soot in the wavelength-range between 450 nm and 700 nm had been determined in a separate campaign, yielding an Angström exponent for absorption of 1.0 (Schnaiter et al., 2006). Taking this Angström exponent the absorption at λ=1064 nm was calculated by extrapolation.

Correlations between absorption coefficients measured with PAS and derived from extinction and scattering measurements by the difference method (DM, Schnaiter et al., 2005) are shown in Figs. 2 and 3 for pure CAST-soot and mixtures of CAST-soot with non-absorbing but scattering sodium nitrate at λ=266 nm and λ=532 nm, respectively. The latter experiments with aerosol mixtures were deduced to see whether PAS has an interference due to strong aerosol scattering, which was not the case. Here, the absorption Angström exponent determined by DM in the 450–700 nm spectral region was used to extrapolate and interpolate the DM deduced absorption coefficients at λ=450 nm and λ=550 nm to the PAS wavelengths at λ=266 nm and λ=532 nm.

Total number concentrations of the aerosols in the chamber were recorded by a condensation particle counter (TSI, CPC 3022A) operated at a flow rate of 0.3 L min^{-1}. Number size distributions were recorded by an aerodynamic particle sizer (APS; TSI, 3321) operated at a flow rate of 5 L min^{-1}. The APS acquires size distributions in the aerodynamic diameter range from 0.5 to 10 μm with a resolution of 32 channels per decade.

2.2 Experimental procedure

At the beginning of each experiment the NAUA chamber was evacuated, flushed, and re-filled with dry synthetic air, resulting in a background particle concentration of about 2 cm^{-3}. All experiments were performed at room temperature and ambient pressure. Mineral dust aerosol was then added to the chamber via the dispersing set-up described above for about 30 min, which led to initial number concentrations between 1300 and 6700 cm^{-3}. During the subsequent measuring phase, the container volume served as aerosol reservoir for the sampling instruments. On the time scale of the experiments, aerosol dilution was the dominant loss process for mineral dust particles which had no significant effect on the specific optical properties of the aerosol. In addition to the online measurements mineral dust samples were collected on Nuclepore filters for analysis by scanning electron microscopy (SEM).

Two sets of experiments have been performed: In a first set the optical properties were quantified by means of extinction measurements solely, together with measurements of the aerosol number concentration and size distribution. In a second set of experiments, the PAS instrument was additionally operated at the NAUA chamber to measure optical absorption coefficients simultaneously to the extinction spectra recordings.

3 Aerosol concentration and size distribution

A series of similar experiments was performed with four Saharan mineral dust samples of different colour and origin. A soil sample from the Northern Sahara, Cairo 2, was collected 70 km northeast of Cairo city from a depth of 0.5 m. The colour of this sample is light yellow to light brown. A wind blown dust sample, Cairo 3, was collected on a flat surface in Cairo city after a dust storm event at 19 March 2002. This sample has a similar colour as Cairo 2. A Sahelian soil sample from Agadez (Niger) and a soil sample from Morocco became available by courtesy of L. Schütz from the University

of Mainz. Compared to the Cairo samples, these samples have a darker appearance and are coloured yellow brown (Agadez) to reddish brown (Morocco).

All samples were sieved to grain size fractions of less than 20 μm, 20 to 75 μm, and greater than 75 μm. Our experiments were performed with the smallest fraction of particles up to 20 μm.

Since the investigated mineral dust samples contain different quantities of fine particles in the smallest fraction, the experiments were conducted at different initial number concentrations. While for the Cairo 2 sample the initial concentration was 6700 cm^{-3}, significantly lower initial concentrations between 1300 cm^{-3} and 2200 cm^{-3} were used for the other dust samples (Table 1).

Since the SEM images revealed a non-spherical, irregular, but compact shape of the dust particles (Figs. 4 to 6), the aerosol mass concentration was determined from the APS measurements by first calculating the volume equivalent sphere diameter d_{st} (Stokes diameter) of the irregularly shaped mineral dust particles

$$d_{st} = \sqrt{\frac{\chi}{\rho_p}}\, d_{ae}$$

from the measured aerodynamic diameter d_{ae}. The particle density ρ_p=2.5 g cm^{-3} was determined by pycnometric analysis of the mineral dust sample. To account for the irregular particle shape we used a dynamic shape factor χ=1.5 which is typical for minerals like quartz and sand dust (Baron and Willeke, 2001). A lognormal size distribution was then fitted to the resulting aerosol size distributions as function of d_{st}. Good representations of the measured size distributions were achieved by this approach especially for the large-diameter tail of the distribution which represents the main contribution to the total aerosol volume. The moments of the fit result, i.e. the count median diameter (CMD), the geometric standard deviation, and the total particle number concentration, were used to calculate the mass concentration of the aerosol taking the particle density given above. Over the duration of an experiment both the CMD and geometric standard deviation remained almost constant. This indicates that

coagulation plays only a minor role in the aerosol system as already mentioned above. For the interpretation of the measured aerosol optical properties it is important to note that comparable CMDs and standard deviations were found for the four investigated mineral dust types (Table 1).

4 Mineralogical composition and analysis

The desert dust samples were characterised in cooperation with the Institute of Material Research (IMF I) at FZK, the division of Water Technology and Geotechnology, Institute of Technical Chemistry (ITC-WGT) of FZK and the Astrophysical Institute of the University of Jena.

The elemental composition of each mineral sample was determined for the dust fraction <20 μm by X-Ray Fluorescence Analysis (XRF, Bruker AXS, SRS 303AS). The samples were tempered for one hour at 1000°C prior to the analysis. For each dust type a sample of 200 mg was analyzed. For the measured elements weight percentages of oxides were calculated (Table 3). Thus, the samples yielded total iron oxide contents between 2.0 and 5.0 wt-%.

In addition to the chemical analysis we investigated the mineral composition by IR spectroscopy and X-ray-powder-diffractometry with Rietveld phase analysis (XRD, Bruker AXS, D8 diffractometer). For IR spectroscopy the dust fraction <20 μm was mixed with KBr powder before the mixture was pressed to a pellet. The XRD analysis was performed directly on a granular sample of the dust fraction <20 μm. Figure 7 shows the IR-spectra of Cairo 2 and Agadez in comparison to the spectrum of the pure clay mineral Montmorillonite. Corresponding absorption bands of sample- and reference-spectra at 500 and 1000 cm^{-1} indicate the presence of related clay minerals in both Saharan samples. In Fig. 8 the spectra of Cairo 2 and Agadez are compared with the spectrum of the pure calcite. While Cairo 2 shows several absorption bands consistent with the spectrum of calcite at 1500 cm^{-1}, 800 cm^{-1} and below 500 cm^{-1} the Agadez sample displays no significant absorption bands at these wavenumbers.

Both methods, IR spectroscopy and XRD analysis, show that all investigated samples contain quartz, feldspars and clay minerals in different compositions. In addition, the samples from Cairo and Morocco contain significant amounts of calcite, dolomite and gypsum.

In our case the XRD was especially applied to identify the iron oxide phases hematite or goethite. Depending on the crystal phase of interest the method has a detection limit of 0.1 to 0.5 wt-% for iron oxides. While the Cairo 2 and Cairo 3 samples showed no detectable iron oxide phases, there are indications for goethite in the Agadez sample in a very low concentration of ~0.2 wt-% which is at the detection limit of the method. Only the Morocco sample contains hematite in a quantifiable concentration of 0.6±0.1 wt-%.

5 Results

UV-VIS extinction spectra are shown in Fig. 9 for the four mineral dusts and pure hematite. As expected from the wavelength-dependent complex refractive index of pure hematite (Sokolik and Toon, 1999) the extinction spectrum of synthetic hematite aerosol differs significantly from that of the investigated natural mineral dusts.

For calculating σ_{ext} the aerosol mass concentration was derived from the measured size distributions. Table 1 gives σ_{ext} at the Nephelometer wavelengths of 450, 550 and 700 nm and the corresponding Angström exponent of extinction in the 450 to 700 nm spectral region. It is obvious from Table 1 and Fig. 9 that σ_{ext} and its wavelength-dependence is not very sensitive to the type of dust. Since in case of mineral dust aerosol the extinction is dominated by scattering, this result reflects the comparable size distributions of the different dust types in the chamber (Table 1). The wavelength-dependent absorption properties of the mineral dust aerosols are expressed as σ_{abs} deduced from PAS measurements and as single scattering albedo (SSA, Table 2). The PAS instrument was only available for measurements with the bright dust sample Cairo 2 and the reddish dust sample from Morocco. At the visible wavelength of λ=532 nm SSAs of 0.99±0.001 and 0.98±0.002 were deduced for the Cairo 2 and

Morocco samples. In contrast to these relatively high SSA values in the visible, quite low values of 0.76±0.02 and 0.63±0.04 were found for the Cairo 2 and Morocco sample in the near-UV at λ=266 nm (Table 2). This strong wavelength-dependence of the SSA reflects the strong wavelength-dependence of the absorption coefficient resulting in Angström exponents as large as 5.3 and 4.2 for the Cairo 2 and Morocco samples. When comparing absorption Angström exponents of mineral dusts which are based on a few sampling wavelengths, one has to keep in mind that the corresponding absorption spectra might have significant band structures (e.g. in case of hematite), which is in contrast to the absorption spectra of soots. For Cairo 2 σ_{abs} increases from 0.02±0.004 $m^2\,g^{-1}$ at λ=532 nm to 0.81±0.16 $m^2\,g^{-1}$ at λ=266 nm and for Morocco from 0.06±0.014 $m^2\,g^{-1}$ at λ=532 nm to 1.1±0.26 $m^2\,g^{-1}$ at λ=266 nm. Additionally for Cairo 2 σ_{abs} was determined at the IR-wavelength λ=1064 nm to be 0.03±0.005 $m^2\,g^{-1}$, with a SSA of 0.99±0.01.

6 Discussion

Although the elemental analysis yielded total iron oxide contents between 2.0 and 5.0 wt-% for all mineral dust samples studied in this work, cf. Table 3, neither hematite nor goethite could be detected by XRD in the Cairo 2 and Cairo 3 samples. In case of the Agadez sample goethite is probably present with a concentration of about 0.2 wt-%. Only the Morocco sample contains hematite in a quantifiable concentration of 0.6 wt-%. Thus, most of total iron content detected by XRF seems to be incorporated in primary silicate minerals. It is known that some of these minerals could also appear dark coloured (http://minerals.gps.caltech.edu).

While Alfaro et al. (2004) found in their dust samples comparable total iron contents in the range of 3.0 to 6.5 wt-%, they assigned the significant amount of 2.8 to 5.8 wt-% of this iron to be present in iron oxide phases. However their iron oxide content was determined according to the method by Lafon et al. (2004) as the difference between total iron and its structural fraction. Structural fraction in this case quantifies the remaining

iron content after applying an adapted reductive extraction method as commonly used in soil science (Lafon et al., 2004). This method provides no structural information about the extractable iron and therefore cannot distinguish between the presence of goethite or hematite in the samples.

For calculating SSAs and specific absorption cross sections Alfaro et al. (2004) determined scattering and absorption coefficients by an integrating nephelometer and a dual wavelength aethalometer. Due to light scattering by particles deposited in the filter matrix of the aethalometer the measured attenuation over-estimates the particle absorption and, therefore, has to be corrected. Alfaro et al. (2004) applied a correction method by Bond et al. (1999) with two experimentally determined correction terms, while using the uncorrected scattering cross sections of the nephelometer. They investigated one Sahelian dust from Niger, one Saharan dust from Tunisia and one dust from China and found SSAs at λ=660 nm of 0.95±0.01, 0.97±0.01 and 0.97±0.01 for these dusts. These values are slightly lower compared to our results (Sect. 5). However, since the SSA is strongly size-dependent (Tegen et al., 1996), this difference might be due to their bimodal dust size distributions with a second mode in the super-micron size range (2.0 to 5.0 μm) in addition to the sub-micron particle mode. The values for σ_{abs} of Alfaro et al. (2004) range between 0.12 and 0.07 $m^2\,g^{-1}$ at 325 nm and between 0.02 and 0.01 $m^2\,g^{-1}$ at 660 nm which is in the same order of magnitude as our results.

Retrievals of remote sensing data by Cattrall et al. (2003) from Saharan dust passages at Dry Tortugas, Florida revealed SSA values across the visible spectral range. At λ=530 nm the SSA specified by Cattrall et al. (2003) is about 0.96±0.2 in good agreement with our results. By comparing their and others retrieval results with SSA model results based on laboratory data of the complex refractive indices of bulk minerals they found that the remotely sensed values result in a significantly weaker dust absorption than model predictions.

At the high-altitude aerosol station Jungfraujoch Coen et al. (2004) measured scattering coefficients with an integrating nephelometer and absorption coefficients with an aethalometer. During Saharan dust events (SDE) they found Angström exponents

of absorption between λ=370 nm and λ=590 nm of 1.5 to 1.8 which were significantly larger than the usual Angström exponents of 1.0 to 1.2 from non-Saharan background aerosol. Reflections on the filter were corrected by an empirical correction factor, which was calculated for different aerosol types by Weingartner et al. (2003). As already mentioned in the previous section the determination of Angström exponents of absorption for our dust samples based on the PAS absorption measurements at λ=532 nm and λ=266 nm results in relatively high values between 4.2 (Morocco) and 5.3 (Cairo 2). These results indicate that there exists a significant wavelength-dependence in the UV-VIS light absorption by mineral dusts.

7 Conclusions

For the quantification of the spectral optical properties of weakly absorbing aerosols, in particular mineral dust, the presented combination of extinction spectroscopy with LOPES and absorption measurements with the multiple-wavelength PAS seems to be very promising. For both investigated mineral aerosols we found SSA values which are comparable to values observed in recent laboratory and field studies. Moreover, the SSA values determined in the present study show a strong wavelength-dependence with a steep decrease from the visible to the near-UV.

The chemical and mineralogical composition of the dust samples was analysed with special regard to the iron oxide phases hematite and goethite. Although we have measured the absorption coefficients of only two mineral dust samples, these first investigations indicate that the presence of iron oxide phases in the dust in already very low concentrations of less than one wt-% might be sufficient to significantly increase absorption cross section of the mineral dust aerosol in the visible and especially in the UV. Further laboratory investigations on pure hematite and clay minerals as well as on external mixtures of both will reveal the dependence of σ_{abs} and SSA on iron oxide content more clearly. Additionally, the PAS instrument will be improved by including another wavelength in the near-UV at λ=355 nm which allows a more reliable determi-

nation of the Angström exponent and a better comparison of our absorption data with other laboratory and field results.

Acknowledgements. This research was funded by Helmholtz-Gemeinschaft Deutscher Forschungszentren as a part of the program "Atmosphere and Climate". Partial funding of the work by the Hungarian OTKA Foundation (TS 49872) and by the Hungarian Ministry of Economy and Transport (GVOP-3.1.1.-2004-05-0302/3.0) is gratefully acknowledged. We thank C. Jäger and H. Mutschke (Astrophysical Institute, University of Jena), who provide the IR-Spectra of the dust samples. At Forschungszentrum Karlsruhe we thank G. Beuchle and H. Bernotat (ITC-WGT) for the XRD-analysis, C. Adelhelm (IMF I) for elemental analysis and G. Scheurig (IMK-AAF) for the SEM pictures. A special thank is addressed to K. Megahed (IMK-AAF) and L. Schütz (Institute for Atmospheric Physics, University of Mainz) for providing the desert dust samples.

References

Alfaro, S. C., Lafon, S., Rajot, J. L., Formenti, P., Gaudichet, A., and Maille, M.: Iron oxides and light absorption by pure desert dust: An experimental study, J. Geophys. Res.-Atmos., 109(D8), D08208, doi:10.1029/2003JD004374, 2004.

Andreae, M. O.: Climate effects of changing atmospheric aerosol levels, in: World Survey of Climatology, 16, Future Climate of the World, edited by: Hendersson-Sellers, A., Elsevier Sci, New York, 341–392, 1995.

Baron, P. A. and Willeke, K.: Aerosol Measurement, Wiley, New York, 2001.

Bond, T. C., Anderson, T. L., and Campbell, D.: Calibration and intercomparison of filter-based measurements of visible light absorption by aerosols, Aerosol Sci. Technol., 30(6), 582–600, 1999.

Cattrall, C., Carder, K. L., and Gordon, H. R.: Columnar aerosol single-scattering albedo and phase function retrieved from sky radiance over the ocean: Measurements of Saharan dust, J. Geophys. Res.-Atmos., 108(D9), 4287, doi:10.1029/2002JD002497, 2003.

Coen, M. C., Weingartner, E., Schaub, D., Hueglin, C., Corrigan, C., Henning, S., Schwikowski, M., and Baltensperger, U.: Saharan dust events at the Jungfraujoch: detection by wavelength dependence of the single scattering albedo and first climatology analysis, Atmos. Chem. Phys., 4, 2465–2480, 2004.

Lafon, S., Rajot, J. L., Alfaro, S. C., and Gaudichet, A.: Quantification of iron oxides in desert aerosol, Atmos. Environ., 38(8), 1211–1218, 2004.

Schnaiter, M., Schmid, O., Petzold, A., Fritzsche, L., Klein, K. F., Andreae, M. O., Helas, G., Thielmann, A., Gimmler, M., Mohler, O. M., Linke, C., and Schurath, U.: Measurement of wavelength-resolved light absorption by aerosols utilizing a UV-VIS extinction cell, Aerosol Sci. Technol., 39(3), 249–260, 2005.

Schnaiter, M. , Gimmler, M., Llamas, I., Linke, C., Jäger, C., and Mutschke, H.: Strong spectral dependence of light absorption by organic carbon particles formed by propane combustion, Atmos. Chem. Phys. Discuss., 6, 1841–1866, 2006.

Sokolik, I. N. and Toon, O. B.: Incorporation of mineralogical composition into models of the radiative properties of mineral aerosol from UV to IR wavelengths, J. Geophys. Res.-Atmos., 104(D8), 9423–9444, 1999.

Tegen, I., Lacis, A. A., and Fung, I.: The influence on climate forcing of mineral aerosols from disturbed soils, Nature, 380(6573), 419–422, 1996.

Veres, A. H., Sarlos, F., Varga, A., Szabo, G., Bozoki, Z., Motika, G., and Gyapjas, J.: Nd : YAG laser-based photoacoustic detection of ozone: Comparison of pulsed and quasicontinuous wave operation and field tests, Spectrosc. Lett., 38(3), 377–388, 2005.

Voigt, S., Orphal, J., Bogumil, K., and Burrows, J. P.: The temperature dependence (203–293 K) of the absorption cross sections of O-3 in the 230–850 nm region measured by Fourier-transform spectroscopy, J. Photochem. Photobiol. A., 143(1), 1–9, 2001.

Voigt, S., Orphal, J., and Burrows, J. P.: The temperature and pressure dependence of the absorption cross-sections of NO2 in the 250–800 nm region measured by Fourier-transform spectroscopy, J. Photochem. Photobiol. A., 149(1–3), 1–7, 2002.

Weingartner, E., Saathoff, H., Schnaiter, M., Streit, N., Bitnar, B., and Baltensperger, U.: Absorption of light by soot particles: determination of the absorption coefficient by means of aethalometers, J. Aerosol Sci., 34(10), 1445–1463, 2003.

Table 1. Specific extinction cross sections, size distribution parameters.

sample	σ_{ext} (m^2/g)			A	N	CMD	sd_g
	450 nm	550 nm	700 nm		cm^{-3}	μm	
Cairo 2	3.6±0.5	3.3±0.4	2.8±0.4	0.56±0.1	6700	0.62	1.42
Cairo 3	3.9±0.4	3.7±0.4	3.2±0.4	0.45±0.1	1300	0.63	1.43
Agadez	4.0±0.4	3.7±0.4	3.2±0.4	0.53±0.1	1400	0.63	1.42
Morocco	3.8±0.4	3.4±0.4	2.9±0.3	0.58±0.1	2200	0.59	1.75

σ_{ext} specific extinction cross section
A Angström Exponent for extinction
N initial number concentration at t=0
CMD count median diameter
sd_g geometric standard deviation

Table 2. Specific absorption cross sections and single scattering albedos.

sample	σ_{abs} m^2/g			SSA		
	266 nm	532 nm	1064 nm	266 nm	532 nm	1064 nm
Cairo 2	0.81±0.16	0.02±0.004	0.03±0.005	0.76±0.02	0.99±0.001	0.99±0.01
Morocco	1.10±0.26	0.06±0.014		0.63±0.04	0.98±0.002	

SSA single scattering albedo
σ_{abs} specific absorption cross section

Table 3. Element analysis of desert sand samples by x-ray fluorescence analysis calculated as oxides (sd=standard deviation).

Elements as oxides	Cairo 2 wt-%	sd	Cairo 3 wt-%	sd	Agadez wt-%	sd	Morocco wt-%	sd
SiO_2	55.2	0.08	62.0	0.06	79.4	0.31	70.22	0.17
Al_2O_3	7.7	0.01	9.4	0.01	11.5	0.06	8.37	0.01
CaO	24.3	0.05	13.9	0.01	0.7	0.01	11.47	0.02
MgO	2.9	0.03	4.7	0.04	0.4	0.00	2.26	0.01
Fe_2O_3	4.5	0.02	5.0	0.02	2.0	0.01	3.63	0.03
K_2O	1.18	0.003	1.7	0.00	3.6	0.01	2.04	0.01
Na_2O	1.1	0.18	1.1	0.01	2.2	0.13	0.52	0.02
P_2O_5	0.2	0.01	0.2	0.00	0.0	0.01	<0.1	
TiO_2	1.4	0.07	1.2	0.02	0.3	0.01	0.81	0.05

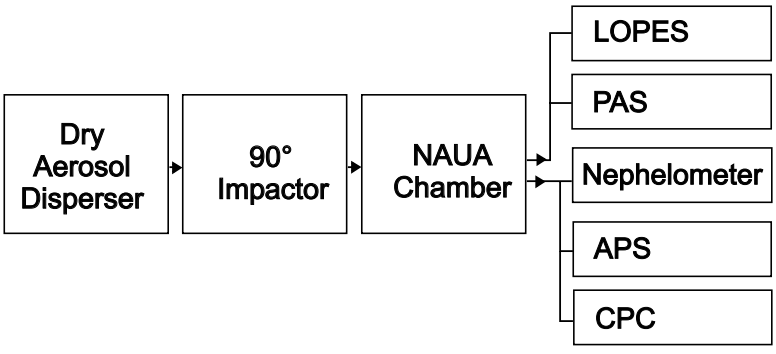

Fig. 1. Experimental setup of mineral dust dispersion, aerosol chamber NAUA and sampling. LOPES: Long Path Extinction Spectrometer, PAS: Photo-acoustic Absorption Spectrometer, APS: Aerodynamic Particle Sizer, CPC: Condensation Particle Counter.

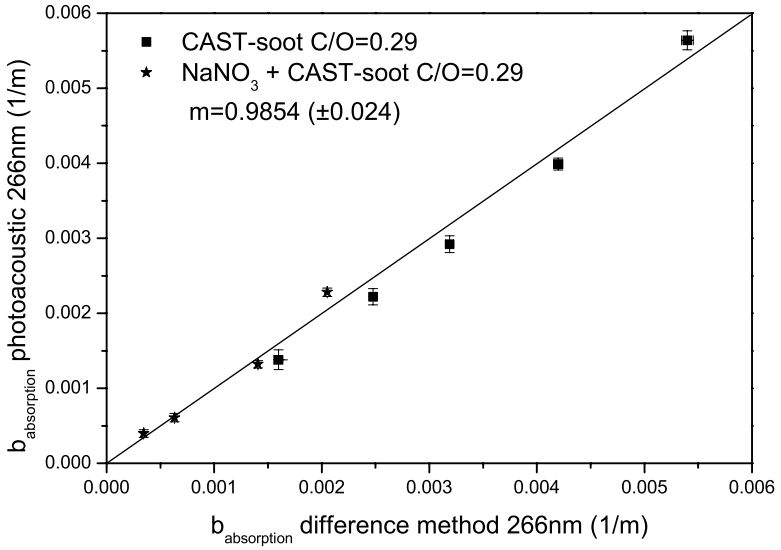

Fig. 2. Comparison of PAS at 266 nm with the difference method (DM) using CAST-soot with a C/O ratio of 0.29.

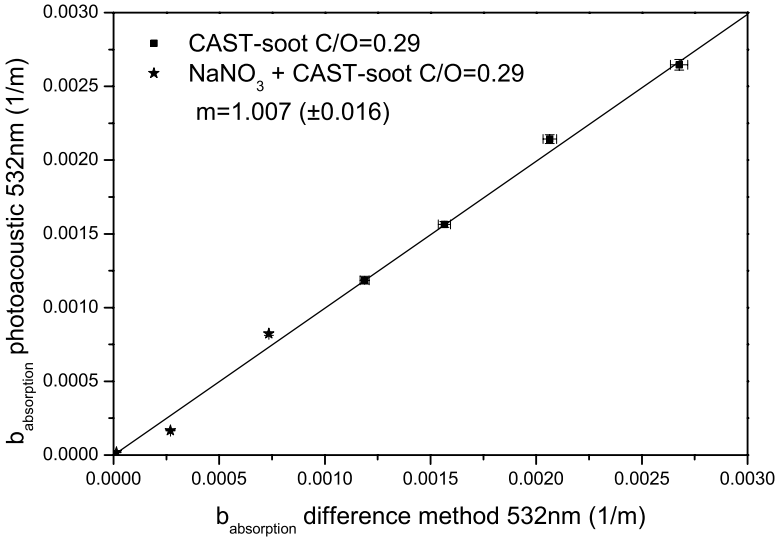

Fig. 3. Comparison of PAS at 532 nm with the difference method (DM) using CAST-soot with a C/O ratio of 0.29.

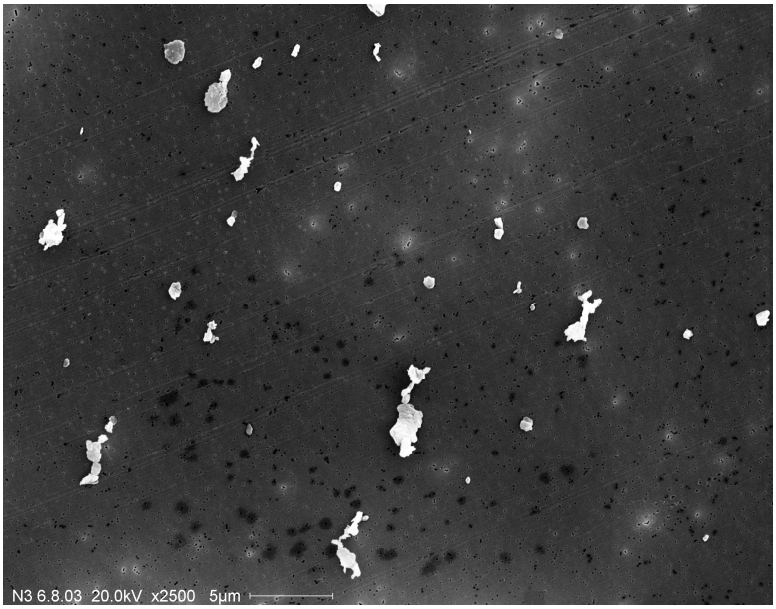

Fig. 4. SEM picture of mineral dust Agadez.

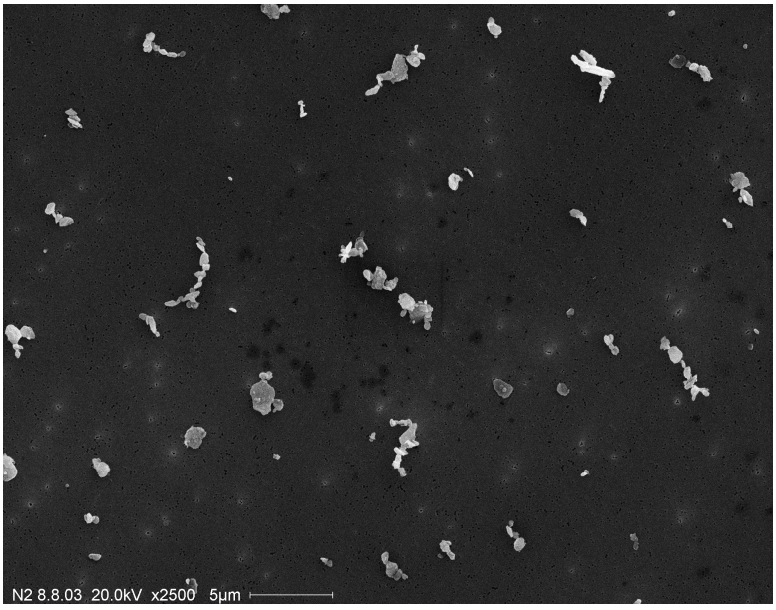

Fig. 5. SEM picture of mineral dust Cairo 2.

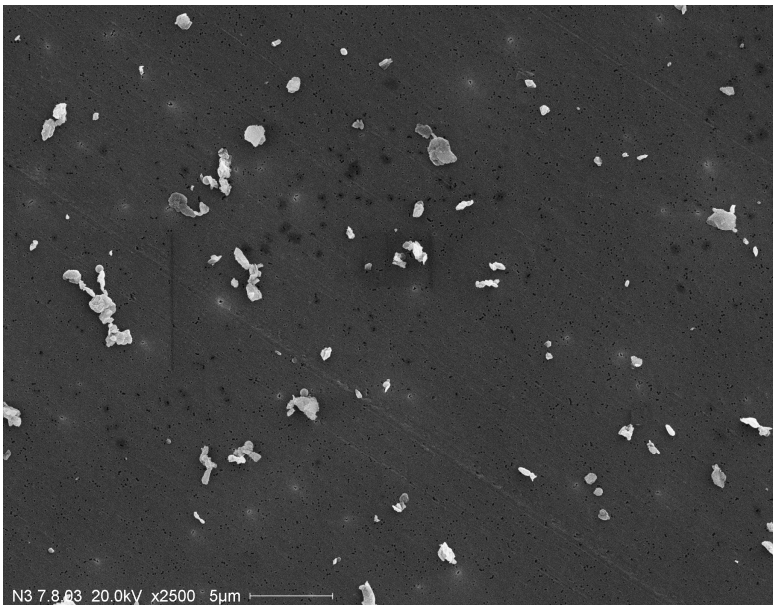

Fig. 6. SEM picture of mineral dust Cairo 3.

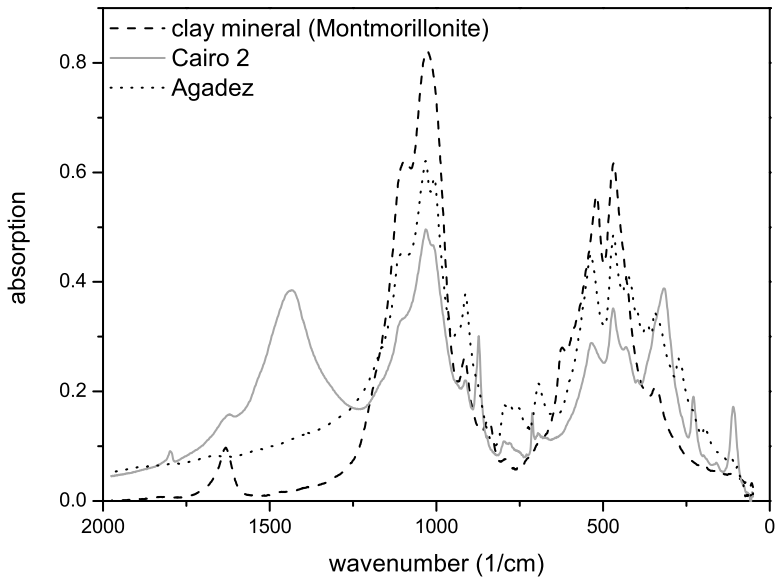

Fig. 7. IR-spectra of mineral dust Cairo 2, Agadez and of the clay mineral Montmorillonite.

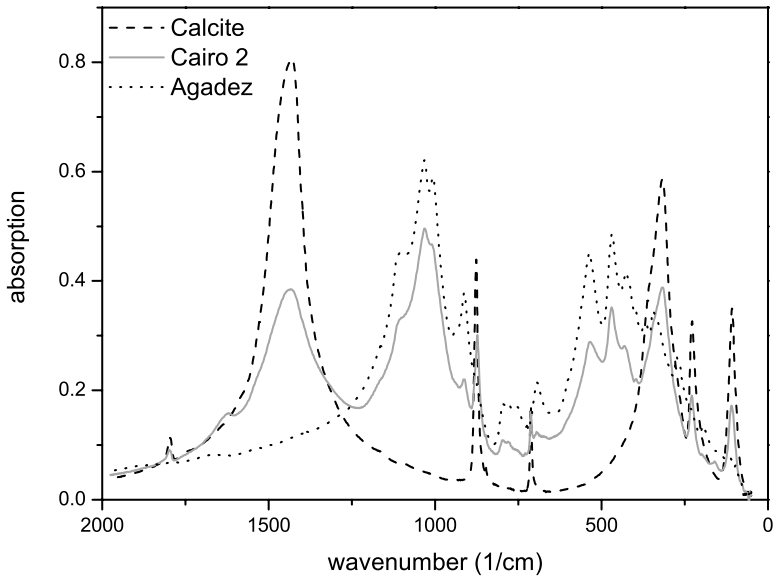

Fig. 8. IR-spectra of mineral dust Cairo 2, Agadez and of calcite.

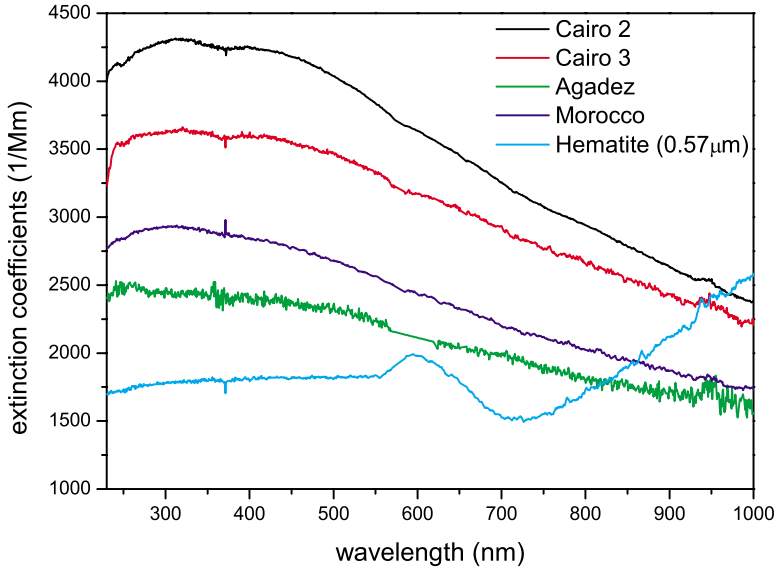

Fig. 9. Extinction spectra of the investigated mineral dust samples and hematite.